IEEE Access
Multidisciplinary | Rapid Review | Open Access Journal

Date of publication xxxx 00, 0000, date of current version xxxx 00, 0000.

Digital Object Identifier 10.1109/ACCESS.2019.DOI

Cooperative relative localization using range measurements without a priori information

ANUSNA CHAKRABORTY[‡], **KEVIN M. BRINK**[*], **RAJNIKANT SHARMA**[‡]

[‡] Dept. of Aerospace Engg., University of Cincinnati, OH, USA
[*] Munitions Directorate, Air Force Research Laboratory, Eglin Air Force Base, FL, USA

Corresponding author: A. Chakraborty (e-mail: anusna90@gmail.com).

This work was funded by the Air Force Research Laboratory Grant No - FA8651-16-1-0001

ABSTRACT The ability for autonomous vehicles to cooperatively navigate, especially in GPS denied environments, is becoming increasingly important. It also requires the ability to initialize, or reinitialize estimation algorithms for cooperative systems on-the-fly in cases where precise *a priori* state information is unavailable. In this paper, we provide a framework that allows estimation of the relative pose and orientation between vehicles in the presence of high initial uncertainty. Effects of cooperation among multiple vehicles exchanging estimates of heading rate and velocity and external sensor measurements are analyzed. A Multi-Hypothesis Extended Kalman Filter (MHEKF) technique is used to initialize pairwise vehicles using range-only measurements. Using solutions identified by the MHEKF algorithm, a joint filter comprising of multiple vehicles is initialized. Sufficient conditions to maintain bounded errors are derived through nonlinear observability analysis using Lie derivatives for the pairwise and the multi-vehicle cases. Using these conditions as passive constraints in the system, simulation and hardware experiments are performed to demonstrate the advantages of using MHEKF when the initial conditions are unreliable. A multi-vehicle testbed for heterogeneous platforms with different sensing modalities is developed to facilitate hardware testing. Improvements in the system performance when cooperation is introduced among vehicles is also highlighted through experiments.

INDEX TERMS Cooperative localization, relative framework, initialization, observability

I. INTRODUCTION

In recent years, the safe operation of autonomous vehicles in the civil and military domain has become an important area of research. Different entities like NASA [1], Uber [2], Hyundai [3] are working towards urban air mobility (UAM) [4, 5, 6] and development of unmanned vehicles traffic management (UTM) [7, 8] systems. Similarly, the ability to deploy unmanned vehicles in hostile environments has been a growing demand for military applications. Autonomous vehicles (manned/unmanned) in the civilian or military domain should be capable of estimating its pose and orientation in the inertial frame, relative to its surrounding, and with respect to other vehicles operating in close proximity [9, 10]. This ability is termed as localization in literature [11, 12, 13, 14, 15, 16]. Currently, localization is dependent on the combination of information from the inertial measurement unit (IMU) and from the global positioning system (GPS). In hostile territory or in urban canyons, GPS availability can be limited, or the quality of information may degrade due to jamming or occlusions. In the absence of reliable GPS, range measurements from ranging radios, ultra-wideband (UWB) sensors, infrared sensors [17, 18], and/or bearing measurements from cameras [19] between vehicles and known points of interest (landmarks) are used with the IMU data for localization.

Relative localization is defined as the process of estimating the relative pose and orientation among vehicles using inter-vehicle measurements with respect to a common reference frame (in this case, the body frame of the vehicle that is measuring). Precise relative localization is a key for safe operation among multiple autonomous vehicles for close coordination and control purposes. Several researchers have investigated relative localization between two vehicles [20, 21, 22]. Two vehicle relative localization accuracy is low and

This article has been accepted for publication in a future issue of this journal, but has not been fully edited. Content may change prior to final publication. Citation information: DOI 10.1109/ACCESS.2020.3035470, IEEE Access

highly dependent on sensing and observability constraints. It has been shown that the localization accuracy can be improved significantly by exploiting cooperation, where vehicles share their local (IMU) and external (camera, LIDAR) information among the group for localization. This is known as cooperative localization (CL) [23, 24, 25, 26]. There are several advantages of CL that include but are not limited to improvement in estimation accuracy, increase in sensing capacity, and decreased chances of single-point failure. In this paper, we focus on the development of relative localization using range-only measurements among multiple cooperating vehicles. Relative framework-based CL was developed by Mishra *et al* [27] to aid the landing of autonomous vehicles on a moving platform using range-only measurements. Araki *et al* [28] developed a range measurement based CL scenario for autonomous driving in a GPS-denied environment.

One of the fundamental issues with range-only or bearing-only relative localization is the issue of filter initialization without a-priori information. The existing literature does not completely address the initialization issues with relative localization, specifically when cooperation is involved. Initialization problem can easily be solved using particle filters. However, particle filters are computationally expensive for on-board implementation on small robots and UAVs [29, 30]. Xue and Schwartz [29] have provided a comparative study on the performance and time complexity of an EKF and a particle filter. Simulation results provided in the paper show that even though the estimation accuracy of the particle filter is better when compared to EKFs for the same conditions, the time complexity to reach a similar performance is high, making it difficult for implementation in real-time applications. On the other hand, Extended Kalman Filter (EKF), an asymptotic observer, is lightweight and provides good state estimates if good a-priori state information is available. Researchers have used a combined approach with multiple EKFs to tackle the initialization.

A Modified Polar Coordinate Extended Kalman Filter (MPEKF) based solution was proposed in [31]. The authors assume knowledge of inter-vehicle bearing measurements to convert the states to be estimated from cartesian to polar coordinates. A bank of filters with multiple range estimates was used to cover the uncertainty in range. The performance of this filter was compared to a particle filter, and the particle filter provided higher estimation accuracy. A modified version of this algorithm was also developed in the same literature called the Range-parameterised EKF (RPEKF), where range measurements are chosen from an interval of $[\rho_{min}, \rho_{max}]$. Although this method provided comparable results to the particle filter, choosing ρ_{min} and ρ_{max}, which influences the performance of the RPEKF as stated by the authors, is dependent on the application, trajectories, agent velocities, to name a few factors. Similarly, Bai and Beard [32] have used a number of EKFs to estimate the relative orientation when relative position measurements are available. In practice, relative position measurements are hardly available for small UAVs. A weighing technique to assign weights to each individual EKF was used, and the estimates and uncertainty calculated for the filter at every point is a weighted average of the estimates from all the filters. This can lead to filter divergence if some filter estimates are far away from the actual estimates. Calculation of the weighted average also increases the computational complexity of the system.

In our recent work, [33], we have proposed a Multi-Hypothesis Extended Kalman Filter (MHEKF) to estimate relative position and relative heading for two vehicles using range-only measurements. Although the Multi-Hypothesis Extended Kalman Filter sounds similar to the Multi Hypothesis Kalman Filter (MHEKF) or more commonly referred to as the Multi Hypothesis Object Tracking EKF (MHOT-EKF), both these techniques have different structures as well as applications. The MHOT-EKF is a technique used for tracking multiple objects and enables efficient tracking even when data association cannot be made, specially in crowded environments [34, 35]. The MHEKF proposed in [33] and further improved upon in this paper is a technique developed to address the issue of initialization of estimation algorithms in the presence of large initial uncertainty or low/none a-priori information, especially for platforms with low processing power and real-time implementation. The initialization problem for the relative position was solved using a-priori noisy heading information in [33]. We used a simple χ^2 elimination technique to identify filters that provided the "best" estimate and prune out filters with large covariances. It has been shown that for a nonlinear system, an EKF does not provide consistent estimates initial conditions are far from the true states [36]. As the EKF cannot perform accurately with high initial uncertainty and the computational complexity of a Particle Filter is higher to achieve similar performance, the MHEKF provides a solution that is accurate, consistent, and can be performed in real-time on platforms with low processing power.

In this paper, we extend the 2-vehicle relative localization work [33] to an N-vehicle cooperative relative localization problem using the concept of MHEKF to initialize an N-vehicle joint filter with no *a-priori* information (no position or heading information is present). The goal of the N-vehicle filter is to cooperatively estimate the relative pose and orientation of the vehicles with respect to the central vehicle using range measurements between vehicles. We use a 2-vehicle pairwise MHEKF filter to initialize the N-vehicle filter without a-priori relative position and relative heading information. Additionally, in this paper, we perform nonlinear observability analysis [37] to investigate the effect of relative motion on the MHEKF initialization. Antonelli *et al.* [38] performed a linear observability analysis for relative localization. Linear observability analysis of nonlinear systems sometimes leads to inaccurate conditions. In [39], observability analysis for bearing-only and relative pose measurements were performed for a pairwise case, and sufficient conditions were discussed based on the system dynamics. In this paper, we derive conditions for minimum and maximum observability as a function of the relative trajectories

among vehicles and obtain conditions for the N-vehicle case. Using these conditions, the concept of Initialization Manuevers (IMs) has been discussed, which can lead to faster identification of the working filter from MHEKF. The effect of system observability on the convergence time for the MHEKF has also been discussed. Furthermore, we have developed a multi-vehicle experimental testbed to validate the MHEKF based cooperative relative localization where we use ultra-wideband (UWB) low-cost Decawave [40] sensors to measure the range between vehicles.

Based on the discussion above, the major contributions of this paper are can be reiterated as follows:

- Development of an N-vehicle cooperative relative localization estimator using range-only measurements among vehicles in the presence of large initial uncertainty.
- Improvement of the Multi-Hypothesis Extended Kalman Filter (MHEKF) technique introduced in [33] by removing a-priori heading information. A rule of thumb while choosing the initial number of filters for the MHEKF has also been provided in the paper, which is a function of the overlap between the 2σ uncertainty ellipses around the different initial points. This is used as a user-input based on the application scenario.
- Nonlinear observability analysis using Lie derivatives has been performed for both the pairwise case and the N-vehicle case that aids in identifying the relative trajectories among vehicles that provide better estimation accuracy.
- A multi-vehicle testbed has been developed where different sensors (UWB decawave, cameras) have been used to perform the cooperative relative localization algorithm

The paper is organized in the following manner. Section II formulates the mathematical definition of the problem. Simulation results are presented in this section to aid in understanding the estimation problem with no a-priori information and the use of the MHEKF algorithm in resolving it is also presented. A nonlinear Observability analysis for the direct and indirect measurements cases are presented in Section III followed by hardware results detailed in Section IV. Conclusions from the paper and possible future work are discussed in V.

II. PROBLEM FORMULATION

Consider N vehicles moving in a horizontal plane as shown in Figure 1. The inertial equations of motion of the i^{th} vehicle is represented using a unicycle kinematic model as

$$\begin{bmatrix} \dot{p_{n_i}} \\ \dot{p_{e_i}} \\ \dot{\psi_i} \end{bmatrix} = \begin{bmatrix} v_i \cos\psi_i \\ v_i \sin\psi_i \\ \omega_i \end{bmatrix} \tag{1}$$

where, v_i and ω_i are the linear and angular velocities of the i^{th} vehicle, $[p_{n_i},\ p_{e_i}]^\top$ is the position vector in the inertial coordinate (NED) frame, ψ_i is the heading angle, and $i \in [1, \cdots, N]$. In the absence of GPS or any global information in the form of landmarks, relative pose estimation provides navigation and path-planning solutions for close coordination and control problems. Using (1), the relative pose between the ith and jth vehicle is obtained by rotation of the inertial frame of the j^{th} vehicle in (1) to the ith vehicle's frame as shown in Figure 1. The relative pose is represented as

$$\begin{bmatrix} p^i_{x_{ji}} \\ p^i_{y_{ji}} \\ \delta^i\psi_{ji} \end{bmatrix} = \begin{bmatrix} \cos\psi_i & \sin\psi_i & 0 \\ -\sin\psi_i & \cos\psi_i & 0 \\ 0 & 0 & 1 \end{bmatrix} \begin{bmatrix} p_{n_j} - p_{n_i} \\ p_{e_j} - p_{e_i} \\ \psi_j - \psi_i \end{bmatrix} \tag{2}$$

where, the ith vehicle is the central vehicle *i.e* the body frame of the vehicle in which the relative pose and heading are calculated. Using (2), the relative pose motion model is derived by taking the time derivative of (2) and the final equations are defined as

$$\begin{aligned} \dot{x}^i_{ji} &= f(x^i_{ji}, u^i_{ji}, \sigma_{u^i_{ji}}) \\ &= \begin{bmatrix} \dot{p}^i_{x_{ji}} \\ \dot{p}^i_{y_{ji}} \\ \delta^i\dot{\psi}_{ji} \end{bmatrix} = \begin{bmatrix} \hat{\omega_i} p^i_{y_{ji}} + \hat{v_j}\cos\delta\psi^i_{ji} - \hat{v_i} \\ -\hat{\omega_i} p^i_{x_{ji}} + \hat{v_j}\sin\delta\psi^i_{ji} \\ \hat{\omega_j} - \hat{\omega_i} \end{bmatrix} \end{aligned} \tag{3}$$

where, $p^i_{x_{ji}}$, $p^i_{y_{ji}}$ and, $\delta\psi^i_{ji}$ are the relative pose of the jth vehicle in the central (ith) vehicle's frame, $\hat{v_j}$ and, $\hat{\omega_j}$ are the noisy odometry measurements from the j^{th} vehicle's onboard navigation system. For relative pose estimation, it is considered that the vehicles are fitted with sensors capable of measuring inter-vehicle range. The sensor model is represented as

$$\begin{aligned} \rho^i_{ji} &= h(x) + \mu_{\rho_{ji}} \\ &= \rho^i_{ji} + \mu_{\rho_{ji}} \\ &= \sqrt{{p^i_{x_{ji}}}^2 + {p^i_{y_{ji}}}^2} + \mu_{\rho_{ji}} \end{aligned} \tag{4}$$

where, $\mu_{\rho_{ji}}$ is zero-mean Gaussian noise with σ_ρ standard deviation. If the vehicles are cooperating, then additional range measurements are present between the j^{th} and k^{th} vehicle where $j, k \in [1, N]$ and $j, k \neq i$. The cooperative range measurement is represented as

$$\rho^i_{jk} = \sqrt{(p^i_{x_{ji}} - p^i_{x_{ki}})^2 + (p^i_{y_{ji}} - p^i_{y_{ki}})^2} \tag{5}$$

where, $p^i_{x_{ji}}, p^i_{x_{ki}}, p^i_{y_{ji}}$ and $p^i_{y_{ki}}$ are all estimated in the i^{th} vehicles frame. Henceforth in the paper, the cases with only direct range (between the i^{th} and j^{th} vehicles where $j \in [1, N]$ and $j \neq i$ and represented by the solid lines in Figure 1) measurements will be referred to as direct measurement localization (DML) and the cases considering the direct and indirect (between the j^{th} and k^{th} vehicles where $j, k \in [1, N]$ and $j, k \neq i$ and represented by the dotted lines in Figure 1) range measurements will be referred to as indirect measurement localization (IML). State estimation of

This article has been accepted for publication in a future issue of this journal, but has not been fully edited. Content may change prior to final publication. Citation information: DOI 10.1109/ACCESS.2020.3035470, IEEE Access

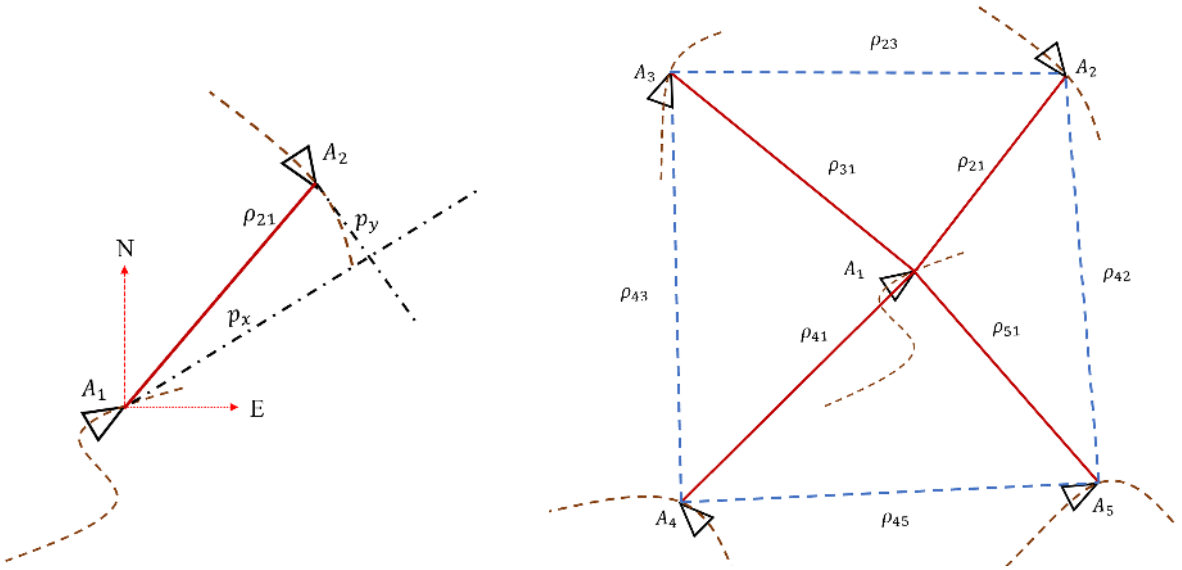

FIGURE 1: Relative Navigation Scenario - Pairwise (only direct measurement - Left) and Multiple (with direct and indirect measurements - Right)

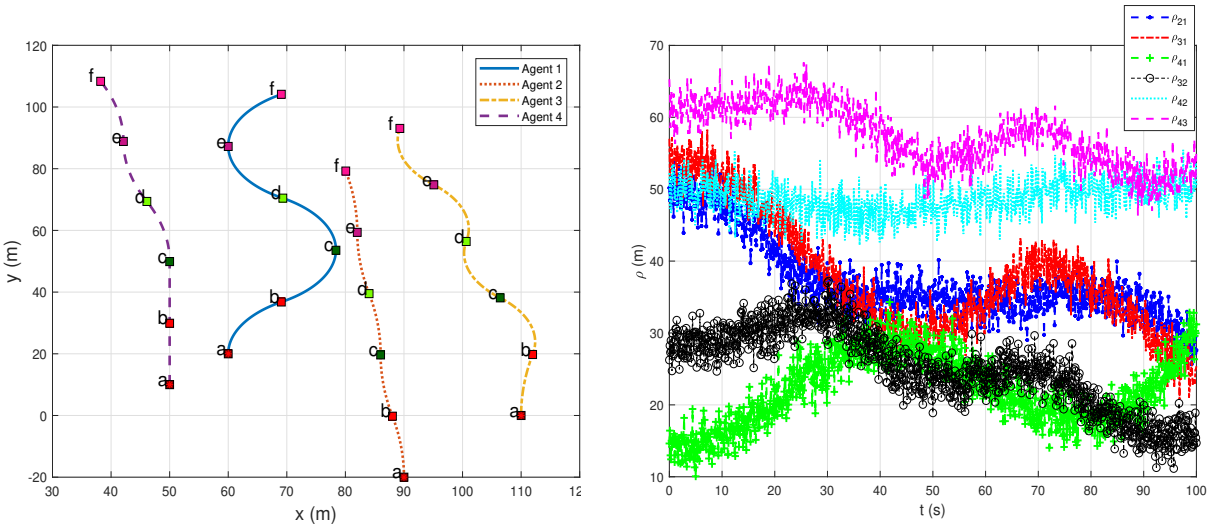

FIGURE 2: Cooperative Relative Navigation Scenario - True Trajectory (Left) and corresponding range measurements (Right)

an N-vehicle system, as shown in Figure 2 using an Extended Kalman Filter (EKF), will provide accurate estimates in the presence of reliable *a-priori* information (low uncertainty). However, for vehicles traveling over long distances without GPS or with the need to re-initialize, the assumption of low initial uncertainty for multiple vehicles is not valid. For example, Figure 3 represents a case of multiple vehicles with high initial uncertainty. The true global trajectories and range measurements of these vehicles are shown in Figure 2. The simulation parameters for this case is presented in Table 1.

The vehicles are moving in an area of $120m$ x $120m$ in Figure 2. A close look at the uncertainty in relative pose between vehicles **1** and **4** in Figure 3 show that the bounds are high. The filter is inconsistent, and these results are commensurate with the behavior among the other vehicle pairs with respect to the central vehicle (omitted from paper). With such high uncertainty and errors of the order of 40m, it is unsuitable for any application. The average uncertainty in $\delta\psi^1_{41}$ is approximately $180°$, which provides no information regarding the relative direction of motion among the vehicle pairs. It is clear from this figure that even when the vehicles have indirect measurements, due to the initial high uncertainty, the errors in the estimates are high, and thus the EKF fails. In [33], the authors solved a pairwise case using MHEKF. An argument can be made regarding the use of geometric overlay of range measurements to initialize

This article has been accepted for publication in a future issue of this journal, but has not been fully edited. Content may change prior to final publication. Citation information: DOI 10.1109/ACCESS.2020.3035470, IEEE Access

Parameter	Multiple - Bad Initialization
Initial pose uncertainty - $p_x^i, p_y^i, \delta\psi^i$	30 m, 30 m, 20 °
Range uncertainty	1 m
Odometry uncertainty - σ_v, σ_ω	0.1 m/s, 0.05 rad/s

TABLE 1: Simulation parameters - Multiple Relative Localization for Figure 3

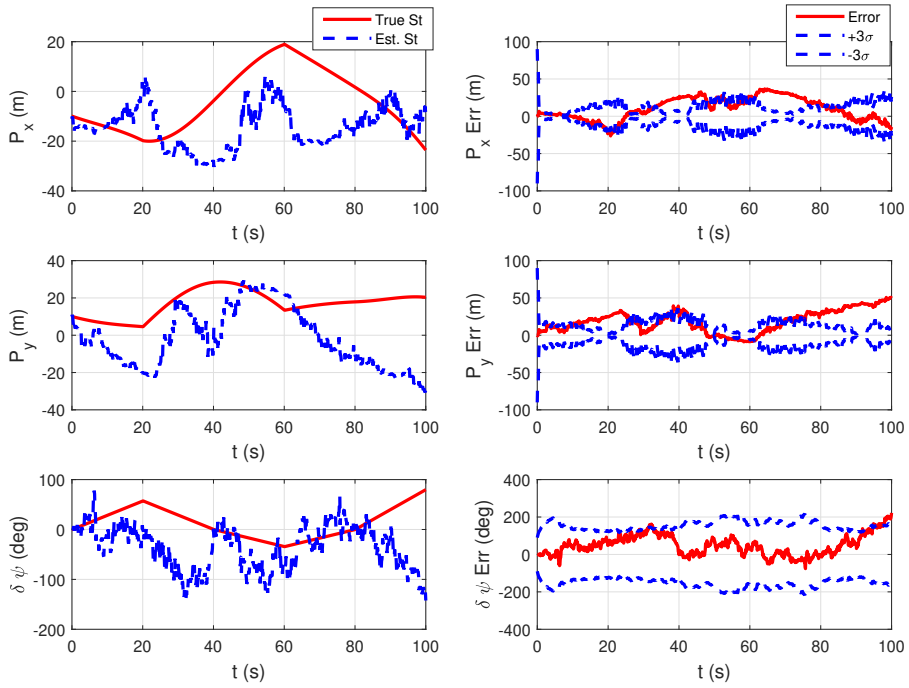

FIGURE 3: Cooperative Relative localization with **high** initial uncertainty (vehicle Pair - 41)

multiple vehicle pairs without the need for multiple filters. This method provides accurate pose and orientation estimates to initialize a system, given all the measurements are available at the same time. Constraints in network bandwidth can cause delays that will reduce the efficiency of this method. Although, in this paper, we assume no data loss or delays in communication and inter-vehicle measurement, all the range information between different pairwise vehicles need not be available at the central vehicle at the same time. Due to the pairwise approach, each vehicle pair is initialized when measurements are received. Thus the system is robust to handle the addition of new vehicles at any time.

One of the drawbacks of using the MHEKF approach is that the vehicles have to be in the sensing and communication range of the central vehicle during the initialization as the relative pose estimation is performed at a central node. A distributed approach solves this problem. However, that reduces the efficiency of the estimator. The advantages and disadvantages of the different approaches are discussed in detail in [41], redand is outside the purview of this paper. Data delays and communication drop-outs can be handled using a batch processing technique which is better equipped than sequential estimators. Using an EKF for the multi hypothesis approach may increase the run time to identify a working filter, but these filters are computationally efficient. In order to use the MHEKF to initialize the N-vehicle filter, it is important to provide a brief summary of the findings from the paper [33]. In [33], the authors use noisy magnetometer readings to initialize the relative heading between pairwise vehicles. In this paper, we assume no knowledge of relative orientation through sensors (internal or external) and initialize it with relative pose thus increasing the robustness of the approach as seen in Section II-A.

A. MULTI-HYPOTHESIS EXTENDED KALMAN FILTER (MHEKF)

For a complete understanding of the MHEKF, it is essential to highlight the main steps for a single EKF. The prediction step of a continuous-discrete EKF can be outlined as

$$\hat{x}^+ = \hat{x}^- + (\frac{T_s}{N_p})\, f(x,u)$$
$$P^+ = P^- + (\frac{T_s}{N_p})\, (FP + PF^T + Q)$$

Here $F = \frac{\partial f}{\partial x}\, f(x,u)$, T_s is the sampling time for integrating the IMU measurements and N_p is the number of prediction steps before a measurement is integrated into the update step.

This article has been accepted for publication in a future issue of this journal, but has not been fully edited. Content may change prior to final publication. Citation information: DOI 10.1109/ACCESS.2020.3035470, IEEE Access

A continuous-discrete EKF [42] is used as it automatically allows for integrating the higher rate of the IMU data as compared to the frequency of the range measurement. When inter-vehicle range measurements are available, we update the filter using the standard equations,

$$\hat{x}^+ = \hat{x}^- + L(\tilde{\rho} - \hat{\rho})$$
$$P^+ = (I - LH)P^-$$

where, $\tilde{\rho}$ is the range measurement received, $\hat{\rho}$ is the predicted measurement from the filter, $H = \frac{\partial h(\hat{x},u)}{\partial x}$ is the measurement Jacobian and L is the Kalman gain. A single filter cannot handle the high uncertainties when initialized away from the truth as seen in Figure 3 and hence we move to a Multi-Hypothesis approach detailed below.

Using range data only, 2π uncertainty is assumed in the relative bearing. A bank of initial guesses is placed on the circumference using the range measurement as the radius while uniformly dividing the circle into N_η evenly spaced initial estimates using Algorithm 1. Figure 4 shows an example where 36 filters are initialized. The choice of the number of filters is dependent on the application. Depending on the overlap percentage *i.e*, how closely the initial points are sampled, an initial start regarding the number of guesses as a function of the 2σ overlap is defined in Algorithm 1. Each filter is represented using solid stars, and the dotted circular trajectories represent the 2σ uncertainty in the relative position. The initial guesses are chosen such that there are two guesses within the uncertainty overlap to ensure that at least a single filter remains consistent throughout the run. The square marks the true relative position between the vehicles, the diamond denotes a filter initialized far away from the truth, and the hexagon denotes a filter spawned close to the true position. Intuitively, the filter initialized close by has a high probability of converging. For every initial p_x, p_y pair, there are N_ψ combinations of $\delta\psi$. In this section, vehicles **1** and **4** are used from Figure 2 to demonstrate the effectiveness of the MHEKF technique. Algorithm 1 summarizes the steps needed to initialize the pairwise MHEKF where N_ψ is the number of evenly placed points for heading initialization, N_η is the number of evenly placed points for position initialization, and $k = \frac{2\pi}{N_\eta}$. The simulation parameters for the MHEKF are listed in Table 2.

Once the algorithm begins, the linear velocity v_i and angular velocity ω_i are exchanged between the central vehicle and the j^{th} vehicle, which are used as inputs to the estimator. This maintains the conditions necessary for EKF convergence, as derived in [36]. As explained in [33], many of the filters initialized via the MHEKF will fail simply because the nonlinearities associated with them are high if they are initialized at points away from the actual initial states as seen in Figure 5. For example, the initial guess highlighted in diamond in Figure 4 starts away from the true relative position and fails as expected. However, other filters will track the system quite well if they start close to the true pose

Algorithm 1 Multi-Hypothesis Extended Kalman Filter - Initialization

Step 1 $\rightarrow$ Circle circumference: $2\pi\rho$
Step 2 $\rightarrow$ Minimum number of circles without overlap: $\tau = \frac{2\pi\rho}{2\sigma} - 1$
Step 3 $\rightarrow$ Round off τ to the nearest even integer
Step 4 $\rightarrow$ Defining overlap% α, number of points: $N_\eta = \tau + 2\alpha\tau\sigma$
for i in 1 - N_η **do**
  for j in 1 - N_ψ **do**
    Step 5 $\rightarrow$ **Initialize** $\dot{p}^i_{x_{ji}} = \rho\cos(\eta_k)$
    Step 6 $\rightarrow$ **Initialize** $\dot{p}^i_{y_{ji}} = \rho\sin(\eta_k)$
    Step 7 $\rightarrow$ **Initialize** $\dot{\delta\psi}^i_{ji} = \frac{2\pi}{N_\psi}$
  end for
end for

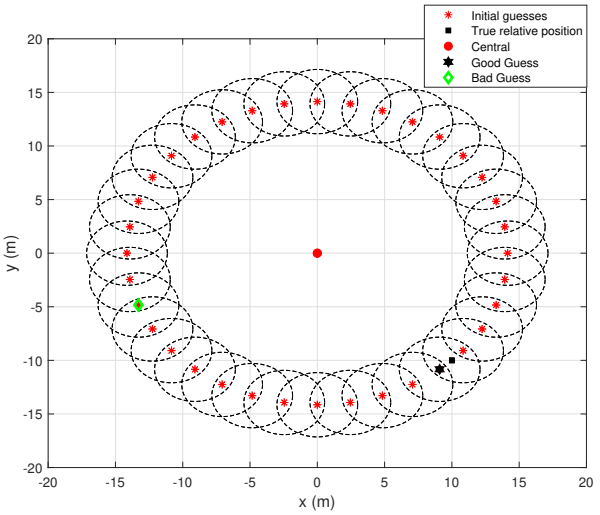

FIGURE 4: MHEKF - Initial guesses (solid star), 2 σ bounds (dotted black lines), and true relative pose (solid black square)

like the initial guess marked as a hexagon in Figure 4. In order to find filters that are close to the true trajectory, we use a simple χ^2 inspired approach. We define $e^k = |\rho - \hat{\rho}|$ and sum the number of times each filter's range residual is below a user-defined threshold. Usually, this threshold is chosen as $3\sigma_\rho$ where σ_ρ is the measurement noise associated with range. Whenever it is below that threshold, a count for that filter is incremented. The larger the χ-count of a filter means the higher chance of that filter converging eventually. The cumulative plot for χ^2 sum for every filter is presented in Figure 5. The filters initialized close to the truth have higher χ-counts as seen with the solid line that corresponds to the initial guess marked as a hexagon. However, the filters initialized far away have low χ-counts are discarded. The χ^2 elimination technique is

$$if \quad |e^k| \leq c\sigma_\rho, \quad then \quad \chi^k = \chi^k + 1 \tag{6}$$

This article has been accepted for publication in a future issue of this journal, but has not been fully edited. Content may change prior to final publication. Citation information: DOI 10.1109/ACCESS.2020.3035470, IEEE Access

Parameter	MHEKF - Simulation
Initial pose uncertainty - $p_x^i, p_y^i, \delta\psi^i$	1 m, 1 m, 6 °
Initial range measurement	14 m
Range uncertainty	1 m
Odometry uncertainty - σ_v, σ_ω	0.1 m/s, 0.05 rad/s
Total number of filters	36

TABLE 2: Simulation parameters - MHEKF for Figs 4- 6

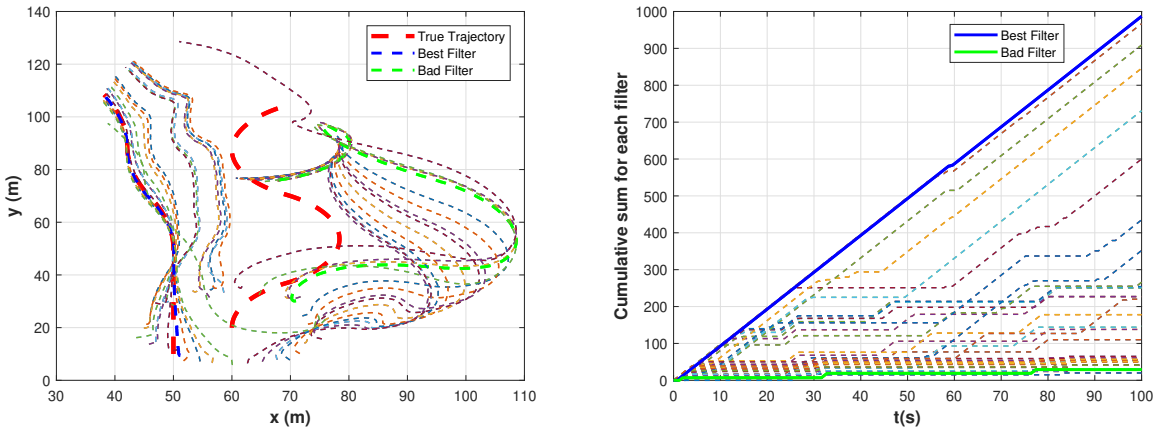

FIGURE 5: MHEKF - All trajectories (Left) & the corresponding Cumulative χ-counts (Right)

As seen from Figure 5, this criteria identifies the filter with the largest χ value, and we use this as our best estimate to initialize the N-vehicle system. Using the elimination technique from (6), the best estimate and one of the bad filters are represented in Figure 6. It is to be noted that the filter with the best estimates on the left does not show a significant improvement in the covariance from the initialization. This clearly shows that the MHEKF is not used to improve the quality of estimates for the best filter but avoids a bad initial guess to be used in the initialization of the N-vehicle system. The best estimates in Figure 6 is from the initial guess marked with a hexagon in Figure 4 whereas the bad filter estimates shown is the guess marked as a diamond. It is seen that the best guess is consistent and observable with tight uncertainty bounds. This technique with a pairwise solution is used to provide decent initial guesses among vehicle pairs (vehicle **4** and vehicle **1**) with smaller uncertainties to start the N-vehicle filter.

In this case, results for a **100** seconds run is shown. The time for the MHEKF to converge is user-defined, depending on the accuracy demanded by the application. However, certain trajectories have been shown to provide a working filter faster than other trajectories. These trajectories are referred to as Initialization Maneuvers (IM). The convergence of the uncertainty bounds is closely related to the observability of the system, which is discussed in detail in Section III. Improving the observability of the system by increasing the relevant information in the estimation aids in identifying the best filter quickly.

Based on the MHEKF technique to initialize vehicles in a pairwise scenario, Figure 7 represents the N-vehicle filter where each of the vehicle pairs is initialized after 20 seconds (represented by the black vertical line). After the 20 second mark, indirect range measurements are added to the estimator (represented by dotted lines). It is clear from Figure 7 that indirect measurements among vehicles aids in faster convergence and improves estimation quality. These indirect measurements add cross-correlation terms in the uncertainty matrix and make it a tightly coupled system that provides consistent and observable estimates. This is also highlighted from Table 3.

The root mean square (RMS) errors in the relative pose and orientation are shown for both the IML and DML cases, and the average p_x and p_y between the vehicles are also included to highlight the performance of the filters. Although both the DML and IML have small RMS errors, it is clear that for every vehicle pair, IML outperforms DML, which is expected. The accurate performance of the filters even when no *a-priori* information is present is due to the pairwise Multi-Hypothesis approach. This light-weight initialization technique identifies the best filter between pairwise vehicles, which have low uncertainty and are consistent. Hence, in this section, we have shown the effectiveness and efficiency of using MHEKF to initialize an N-vehicle filter with no *a-priori* information. The algorithm followed for the localization of the N-vehicle filter is similar to [25]. The information exchange in the system is represented in Figure 8. The pairwise vehicles are initialized using MHEKF, and after identifying the best filter, this information, along with the individual vehicles' odometry and range measurements, are

This article has been accepted for publication in a future issue of this journal, but has not been fully edited. Content may change prior to final publication. Citation information: DOI 10.1109/ACCESS.2020.3035470, IEEE Access

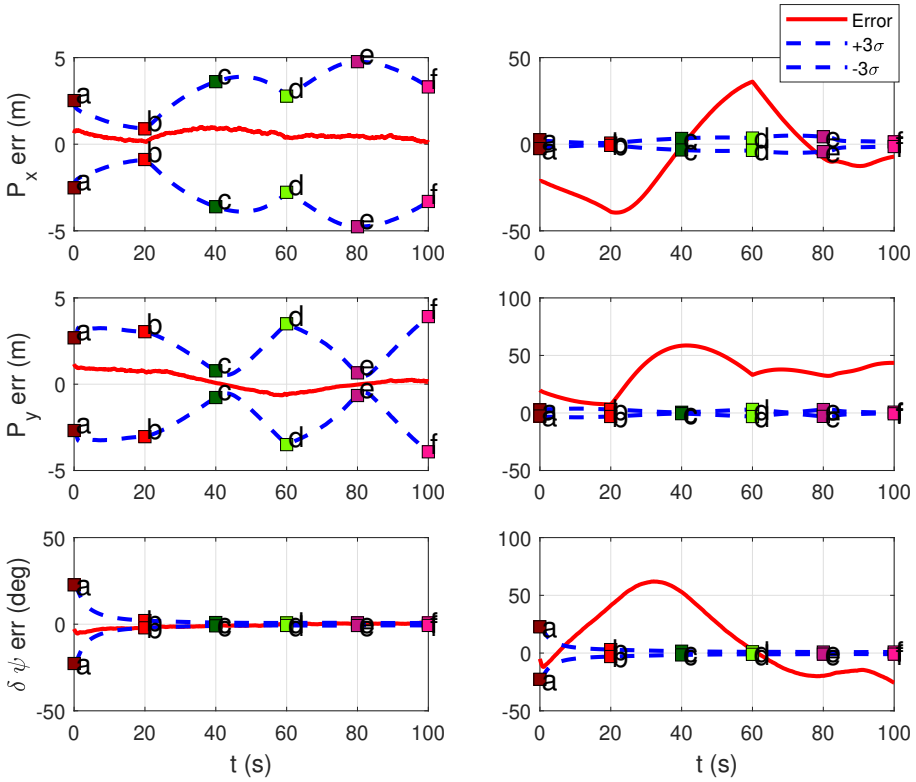

FIGURE 6: MHEKF - Best Filter Errors (Left) and Bad filter errors (Right)

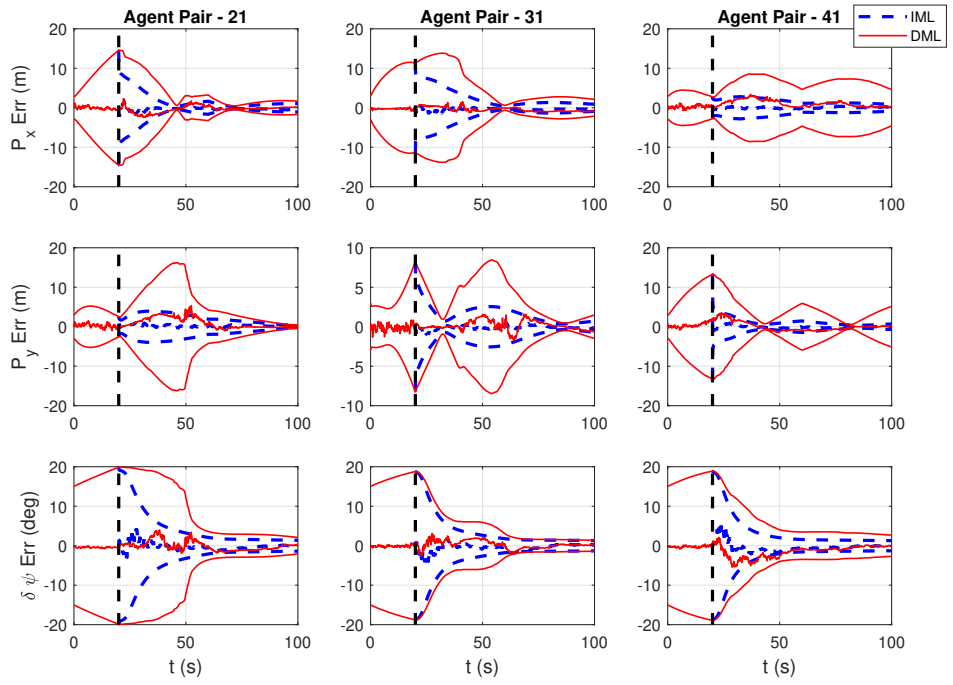

FIGURE 7: Error with 3σ bounds for a multi-vehicle scenario. The trajectory followed is the same as Figure 2. The dotted line indicate IML and the solid lines indicate DML

This article has been accepted for publication in a future issue of this journal, but has not been fully edited. Content may change prior to final publication. Citation information: DOI 10.1109/ACCESS.2020.3035470, IEEE Access

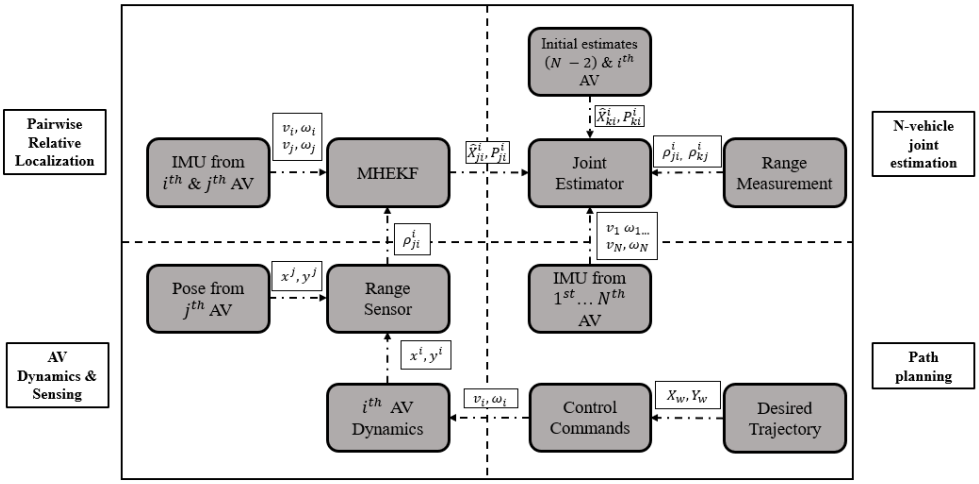

FIGURE 8: Block diagram for Cooperative Relative Localization

used as inputs to the N-vehicle filter. Since the MHEKF is a filtering problem, convergence rate and quality of estimation are dependent on the quality of measurements (range in this case) received, which is closely tied to the observability of the system. The system described in (3) is nonlinear, and Lie derivatives [37] are used to provide a thumb rule in choosing trajectories that makes the system observable in Section III.

III. OBSERVABILITY ANALYSIS

As discussed in Section II, pairwise MHEKF can be used to seed a multi-vehicle system with no *a-priori* information. EKF can be described as an asymptotic observer, and the boundedness on the error in its estimates is tied to system observability. The system defined in (3) is a nonlinear model with range measurement between pairwise vehicles and non-linear observability analysis using Lie derivatives [37] is performed to determine conditions that will keep the system observable such that the uncertainty limits are bounded and decreases over time. A general nonlinear system with states X and inputs $u = [v_i, \omega_i]^\top$ can be defined as

$$\begin{aligned}\dot{X} &= f(X,u) \\ &= \sum_{i=1}^{N} f_{v_i}(X)V_i + \sum_{i=1}^{N} f_{\omega_i}(X)\omega_i \end{aligned} \tag{7}$$

where N is the total number of vehicles in the system, f_{v_i} and f_{ω_i} are the different system models when excited by solitary inputs not dependent on each other. In the pairwise relative localization case, the inputs to the system are $U = [v_i, \omega_i, v_j, \omega_j]^\top$. Based on (7), the system can be represented as $\dot{X} = f_{v_i}v_i + f_{\omega_i}\omega_i + f_{v_j}v_j + f_{\omega_j}\omega_j$ where the different models are

$$f_{v_j} = \begin{bmatrix}\cos\delta\psi^i_{ji}, & \sin\delta\psi^i_{ji}, & 0\end{bmatrix}^\top \tag{8}$$

$$f_{v_i} = \begin{bmatrix}-1, & 0, & 0\end{bmatrix}^\top \tag{9}$$

$$f_{\omega_j} = \begin{bmatrix}0, & 0, & 1\end{bmatrix}^\top \tag{10}$$

$$f_{\omega_i} = \begin{bmatrix}p^i_{y_{ji}}, & -p^i_{x_{ji}}, & -1\end{bmatrix}^\top \tag{11}$$

$$\tag{12}$$

The n^{th} order Lie derivatives for a nonlinear system with the motion model $\dot{X} = f(X,u)$ and measurement model $z = h(X) = [h_1(X)\ h_2(X)\ \cdots\ h_n(X)]^\top$ is defined as

$$L^n_f(h) = \frac{\partial}{\partial x}[L^{n-1}_f(h)]\dot{x} \tag{13}$$

where, the zeroth order Lie derivative is defined as $L^0_f(h) = h$. A matrix G can be defined as

$$G = \begin{bmatrix} L^0_f(h_1) & \cdots & L^0_f(h_n) \\ \vdots & \ddots & \vdots \\ L^{n-1}_f(h_1) & \cdots & L^{n-1}_f(h_n) \end{bmatrix} \tag{14}$$

The gradient of matrix G defined in (14) is the observability matrix of the system ($O = \Delta G$). Using (13) and (14), the Lie derivatives for the system defined in (3) is defined as

-	**Avg. p_x (m)**	**IML - p_x (m)**	**DML - p_x (m)**	**Avg. p_y (m)**	**IML - p_y (m)**	**DML - p_y (m)**	**IML - $\delta\psi$ (deg)**	**DML - $\delta\psi$ (deg)**
p_{21}	-25.20	0.43	0.81	-18.06	0.38	1.47	0.82	1.11
p_{31}	-8.42	0.47	0.63	-31.01	0.32	0.60	0.94	0.93
p_{41}	-3.78	0.28	1.23	17.06	0.43	1.08	1.12	1.88

TABLE 3: Cooperative relative localization - RMS Errors (sim)

$$
\begin{aligned}
L_f^0(h) &= \rho = \sqrt{({p^i_{x_{ji}}}^2 + {p^i_{y_{ji}}}^2)} \\
\nabla L_f^0(h) &= \frac{\partial \rho}{\partial x} = \begin{bmatrix} \frac{p^i_{x_{ji}}}{\rho^i_{ji}} & \frac{p^i_{y_{ji}}}{\rho^i_{ji}} & 0 \end{bmatrix} \\
L^1_{f_{v_j}}(h) &= \nabla L_f^0(h) f_{v_j} = \begin{bmatrix} \frac{p^i_{x_{ji}}}{\rho^i_{ji}} \cos\delta\psi^i_{ji} + \frac{p^i_{y_{ji}}}{\rho^i_{ji}} \sin\delta\psi^i_{ji} \end{bmatrix}
\end{aligned} \tag{15}
$$

$$
\begin{aligned}
L^1_{f_{v_i}}(h) &= \nabla L_f^0(h) f_{v_i} = -\frac{p^i_{x_{ji}}}{\rho^i_{ji}} \\
L^1_{f_{\omega_j}}(h) &= \nabla L_f^0(h) f_{\omega_j} = 0 \\
L^1_{f_{\omega_i}}(h) &= \nabla L_f^0(h) f_{\omega_i} = 0
\end{aligned} \tag{16}
$$

The observability matrix O is defined using (14) as

$$
\begin{aligned}
O &= \begin{bmatrix} \nabla L_f^0(h), & \nabla L^1_{f_{v_j}}(h), & \nabla L^1_{f_{v_i}}(h) \end{bmatrix}^\top \\
&= \begin{bmatrix} \frac{p^i_{x_{ji}}}{\rho^i_{ji}} & \frac{p^i_{y_{ji}}}{\rho^i_{ji}} & 0 \\ \frac{p^i_{y_{ji}} J^-}{{\rho^i_{ji}}^{3/2}} & -\frac{p^i_{x_{ji}} J^-}{{\rho^i_{ji}}^{3/2}} & \frac{J^-}{\rho^i_{ji}} \\ -\frac{{p^i_{y_{ji}}}^2}{{\rho^i_{ji}}^{3/2}} & \frac{p^i_{x_{ji}} p^i_{y_{ji}}}{{\rho^i_{ji}}^{3/2}} & 0 \end{bmatrix}
\end{aligned} \tag{17}
$$

where, $J^- = p^i_{y_{ji}} \cos\delta\psi^i_{ji} - p^i_{x_{ji}} \sin\delta\psi^i_{ji}$. The Row Reduced Echelon Form (RREF) of O from (17) is calculated as

$$
U_{rref} = \begin{bmatrix} 1 & 0 & 0 \\ 0 & 1 & 0 \\ 0 & 0 & 1 \end{bmatrix} \tag{18}
$$

U_{rref} satisfies the properties of a RREF matrix, where the leading coefficient in one row is always right of the leading coefficient in the preceding row. The rank of U_{rref} matrix from (18) is 3 for the pairwise relative localization case, which is a full rank system. For a general relative localization algorithm where every vehicle has 3 states each, the full rank redof the system is $3(N-1)$. An interesting observation from (15) is that space spanned by the velocity excitation is nonzero, whereas the angular velocity spans a null space and does not directly contribute to the observability of the system. From (17), it is clear that in a pairwise case, the linear velocity of both the vehicles has to be nonzero for the system to remain observable. Optimizing the relative heading between the pairwise vehicles can aid in path planning algorithms to increase the information flow in the system and ensure system observability. The determinant of the observability gramian ($O^\top O$) provides insight regarding the types of trajectories that improve system observability based on range measurement. Using (17), the determinant of the observability gramian is

$$
\Delta O^\top O = \frac{{p^i_{y_{ji}}}^2}{{\rho^i_{ji}}^3} (p^i_{y_{ji}} \cos\delta\psi^i_{ji} - p^i_{x_{ji}} \sin\delta\psi^i_{ji})^2 \tag{19}
$$

Taking the first derivative of (19) with respect to $\delta\psi^i_{ji}$ and setting it to zero provides the roots of (19) which can either be a maxima or a minima. The roots of (19) are

- $p^i_{y_{ji}} = 0$
- $\delta\psi^i_{ji} = tan^{-1}(\frac{p^i_{y_{ji}}}{p^i_{x_{ji}}})$
- $\delta\psi^i_{ji} = tan^{-1}(\frac{-p^i_{x_{ji}}}{p^i_{y_{ji}}})$

It is clear that when $p^i_{y_{ji}} = 0$, the determinant is minimized. In order to find the roots which maximize and the roots which minimize (19), the second order derivative of (19) is calculated. The second order differential of (19) is given as

$$
\frac{\partial^2 \Delta O^\top O}{\partial \delta^i \psi^2} = -\frac{2{p^i_{y_{ji}}}^2}{{\rho^i_{ji}}^3} [(J^-)^2 - (J^+)^2] \tag{20}
$$

where,

$$
\begin{aligned}
J^- &= p^i_{y_{ji}} \cos\delta\psi^i_{ji} - p^i_{x_{ji}} \sin\delta\psi^i_{ji} \\
J^+ &= p^i_{y_{ji}} \sin\delta\psi^i_{ji} + p^i_{x_{ji}} \cos\delta\psi^i_{ji}
\end{aligned}
$$

Substituting $\delta\psi^i_{ji} = tan^{-1}(\frac{p^i_{y_{ji}}}{p^i_{x_{ji}}})$ in (20), we get $\frac{\partial^2 \Delta O^\top O}{\partial \delta^i \psi^2} = \frac{2{p^i_{y_{ji}}}^2}{\rho_{ji}}$ and with $\delta\psi^i_{ji} = tan^{-1}(\frac{-p^i_{x_{ji}}}{p^i_{y_{ji}}})$ in (20), $\frac{\partial^2 \Delta O^\top O}{\partial \delta^i \psi^2} = -\frac{2{p^i_{y_{ji}}}^2}{\rho^i_{ji}}$. Hence, ${\delta\psi^i_{ji}}^{min} = tan^{-1}(\frac{p^i_{y_{ji}}}{p^i_{x_{ji}}})$ drives the observability of the system towards the minima and ${\delta\psi^i_{ji}}^{max} = tan^{-1}(\frac{-p^i_{x_{ji}}}{p^i_{y_{ji}}})$ towards the maxima condition. This is shown in Figure 9 where if the j^{th} moves along the line joining the two vehicles then the information available in the system is minimized and if it moves perpendicular to the line joining the two vehicles, the information in the system is maximized.

It was previously discussed in Section II that the time taken for the MHEKF to identify the best filter depends on several factors, the most important being the relative trajectories of the vehicles. The effect of the relative trajectories among vehicles on the system observability, which determines the convergence rate of the uncertainty bounds, is clear from (19). In order to initialize a system, the time taken to determine a working filter is an essential parameter

This article has been accepted for publication in a future issue of this journal, but has not been fully edited. Content may change prior to final publication. Citation information: DOI 10.1109/ACCESS.2020.3035470, IEEE Access

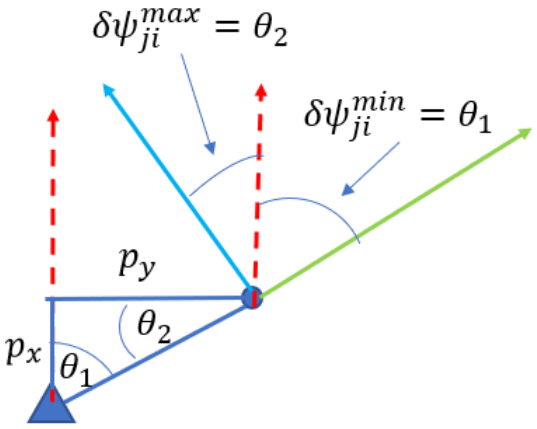

FIGURE 9: Roots of the observability gramian explained geometrically $\theta_1 = tan^{-1}(\frac{p^i_{y_{ji}}}{p^i_{x_{ji}}})$ and $\theta_2 = tan^{-1}(\frac{-p^i_{x_{ji}}}{p^i_{y_{ji}}})$

dependent on the measurements received. It is to be noted that true vehicle states are used to calculate the observability gramian. Conditions required to maintain an observable system are determined as a pre-processed quantity, and hence true states are used.

Figure 10 represents the variation of range measurement ρ, determinant of the observability gramian $\Delta O^\top O$, the information in the system P^{-1} and the cumulative χ-count of all filters initialized in the system with respect to the trajectories. The left column represents two vehicles following circular trajectories in opposite directions, which is clear from the range measurement, which increases and decreases periodically. As expected, based on the range measurement, the observability gramian also follows a cyclic nature. However, there are several points where $\Delta O^\top O = 0$. The information in the system, which is the inverse of the uncertainty, also shows several different minima and maxima. The right column shows pairwise vehicles (vehicles **1** and **4**) from Figure 2 following spline trajectories. The changes in range measurement are smoother and gradual in this case.

$\Delta O^\top O$ reveals an interesting pattern. Although there are different maxima and minima, the area covered is higher than the circular trajectory case (on the left), and this behavior is reflected in the information plot where each of the maxima is higher than the previous peak, and the number of minima is less. This effect is also reflected in the cumulative χ-count plots for both the different sets of trajectories. On the left, it is clearly seen that even around the **80** sec. mark, there are a number of filters with high χ-counts. Most of these filters, however, do not qualify as the "best" filter as their slope reduces near the **100** sec. mark. This behavior is most likely because these filters are inconsistent. As stated in Section I, inconsistent, or over-confident behavior in an EKF is caused by high nonlinearities in the system due to incorrect modeling. As the EKF linearized the system by calculating jacobians, so the jacobians of the filters initialized at points far away from the truth are not calculated near the equilibrium points and hence exhibit behavior that is not accounted for in the system model [43].

In this case, it is difficult to identify the best filter with shorter initialization times. The cumulative χ-counts on the right show that even after the **20** sec. mark, there are 4 distinct filters, and each of these filters performs well till the **100** sec. mark. It has been verified through numerous simulation and hardware experiments, including Monte-Carlo runs, that these filters with the highest χ-count are consistent. So any of these 4 filters (for this case) can be used for the initialization of the larger filter. Information from these filters can also be fused using techniques like covariance intersection [44]. Since the information and the uncertainty bounds for these 4 filters are almost the same, in this case, we have chosen one of the filters for the N-vehicle initialization. So it is clear that if pairwise vehicles follow this trajectory, the best filter is identified within a smaller time frame. The time frame to use an MHEKF to identify a filter is a user-dependent parameter. In terms of practical feasibility, a small window of time to identify a good filter is desirable. In this case, the "smaller time frame" is meant as a comparison between the two different trajectory cases shown in Figure 10. So, the time frame of the spline trajectories to identify a good filter is smaller as compared to the time taken if the vehicles follow circular trajectories. This result is also verified from the information and range measurement plots for the two cases, which have been discussed in this section. Such trajectories which reduce the initialization time effectively pruning out inconsistent and/or unobservable filters within smaller time frames can be referred to as initialization maneuvers (IM). The goal of any optimization algorithm will, therefore, be to generate IMs where minimizing initialization time is one of the key constraints. From (19), we show conditions to maintain observability between pairwise vehicles. So (19) shows the conditions that can be utilized in generating trajectories for the pairwise case in MHEKF to provide a consistent filter faster. In this paper, as we solve an N-vehicle filter, indirect measurements (represented by the dotted lines in Figure 1) are also included in calculating the observability gramian. The system can be defined with each input as in (15) where the individual manifolds are:

$$f_{v_j} = [\cos\delta\psi^i_{ji},\ \sin\delta\psi^i_{ji},\ 0,\ \cdots\ \cos\delta\psi^i_{Ni},\ \sin\delta\psi^i_{Ni},\ 0]^\top \tag{21}$$

$$f_{v_i} = [-1,\ 0,\ 0,\ \cdots\ 0,\ 0,\ 0]^\top \tag{22}$$

$$f_{\omega_j} = [0,\ 0,\ 1,\ \cdots 0,\ 0,\ 1]^\top \tag{23}$$

$$f_{\omega_i} = [p^i_{y_{ji}},\ -p^i_{x_{ji}},\ -1,\ \cdots\ p^i_{y_{Ni}},\ -p^i_{x_{Ni}},\ -1]^\top \tag{24}$$

$$\tag{25}$$

The observability matrix is similar to the pairwise case (17) based on the number of cooperating measurements among the vehicles. For a **3** vehicle system with one cooperating measurement, the RREF matrix is defined as

This article has been accepted for publication in a future issue of this journal, but has not been fully edited. Content may change prior to final publication. Citation information: DOI 10.1109/ACCESS.2020.3035470, IEEE Access

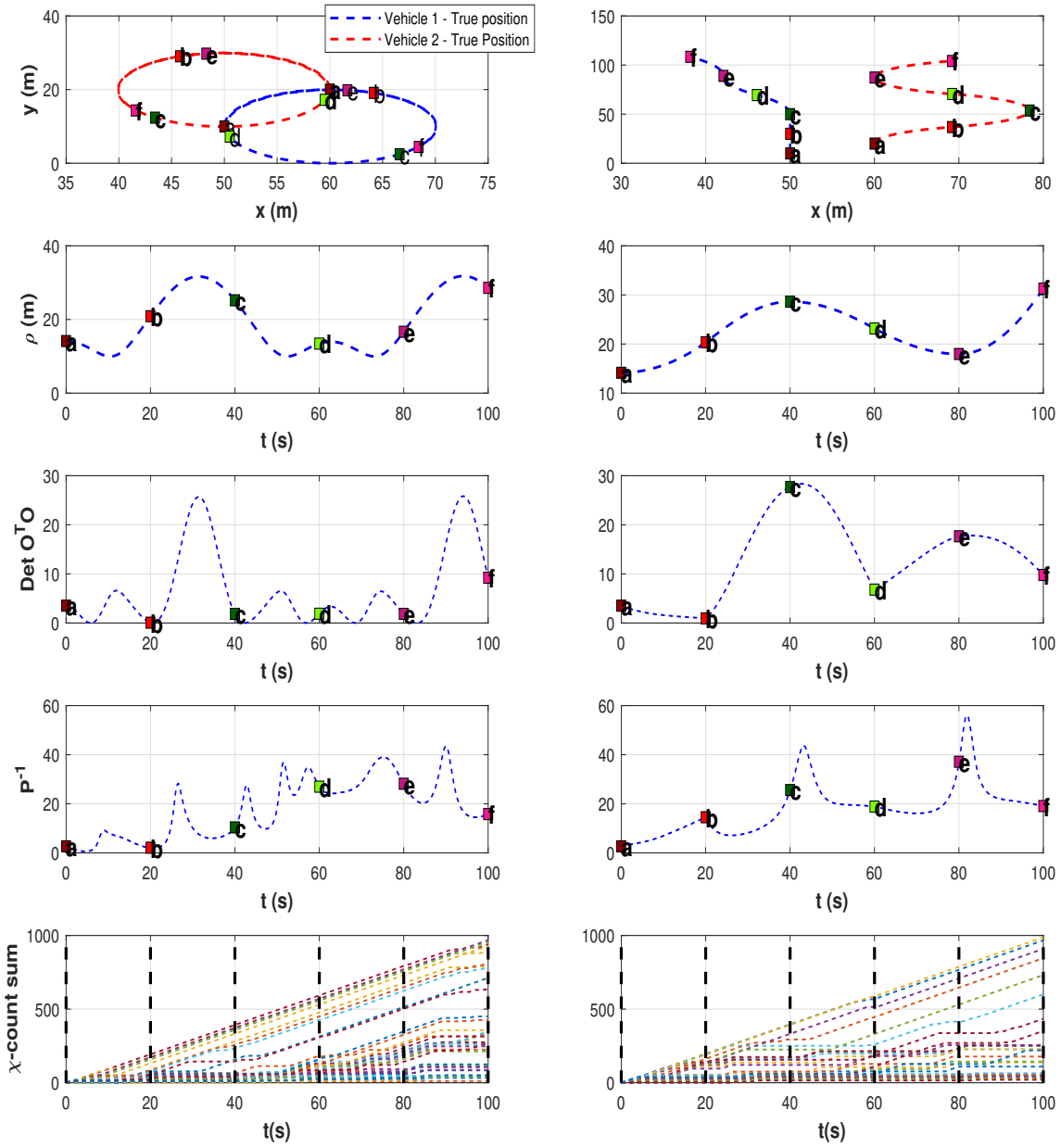

FIGURE 10: Observability as a factor in determining trajectories with faster convergence time to identify best filter in MHEKF

This article has been accepted for publication in a future issue of this journal, but has not been fully edited. Content may change prior to final publication. Citation information: DOI 10.1109/ACCESS.2020.3035470, IEEE Access

$$U_{rref} = \begin{bmatrix} 1 & 0 & 0 & -1 & 0 & \Delta p_y \\ 0 & 1 & 0 & 0 & -1 & -\Delta p_x \\ 0 & 0 & 1 & 0 & 0 & -1 \\ 0 & 0 & 0 & 0 & 0 & 0 \\ 0 & 0 & 0 & 0 & 0 & 0 \\ 0 & 0 & 0 & 0 & 0 & 0 \\ 0 & 0 & 0 & 0 & 0 & 0 \end{bmatrix} \quad (26)$$

where, $\Delta p_x^i = p_{x_{ji}}^i - p_{x_{ki}}^i$, $\Delta p_y^i = p_{y_{ji}}^i - p_{y_{ki}}^i$, $j, k \, \epsilon [2, N]$, $j, k \neq i$ and $i = 1$ is the central vehicle. From (26), it is clear that the rank of the system is $3(N-2)$, which makes it a rank **3** deficient system with only indirect range measurements. Using the concepts developed in [26] by converting the N-vehicle problem into a 2-level tree, the system becomes full rank when at least one vehicle is present in the sensing region of the central vehicle. The rank of the system is $3(N-2)$ from the indirect measurement and **3** for the direct measurement between the central and j^{th} vehicle. The total rank of the system is $3(N-2) \, + \, 3 \, = 3(N-1)$, which is the full rank for a cooperative relative localization problem. As part of the future work, controllers with optimized relative heading can be designed to maintain these conditions to ensure maximum observability in the system. Based on the simulation results in Section II, hardware experiments were also conducted to verify the performance of the MHEKF and the N-vehicle in the relative navigation problem, and the results are provided in Section IV.

IV. HARDWARE SETUP AND RESULTS

A multi-vehicle testbed with different sensing modalities was developed for experimental verification. Figure 11 represents a simplified image of the testing platform with 3 robots. The number of robots in the system is variable and heterogeneous robots can be used for testing different algorithms. One of the main features of this testing platform is the seamless integration of different types of sensors. Experiments for this paper was performed using 3 kobuki-base turtlebots [45] fitted with Ultra Wide Band (UWB) range sensors called Decawave (dwm1001) [40]. The turtlebots come with several pre-existing Robot Operating System (ROS) packages that allow end-users to directly read and visualize the IMU data from the robot. With the Decawave sensors, this setup provides a means to directly read range measurements into ROS and provide appropriate control commands in the form of linear and angular velocity. The robots are fitted with gigabyte Brix computers, which is an onboard **i5** computer capable of performing complex operations. These computers are powered by an external power bank that can prevent voltage surges.

The experiment was performed in the presence of 12 Optitrack Motion capture (Mocap) cameras. The Mocap system acts as an indoor GPS and is used for comparison. As seen from Figure 12, the robots are fitted with silver markers on the top plate. The infrared cameras can detect these markers and with the help of custom templates unique to each robot, provide the true position, velocity and heading with respect to the Mocap room area. Using nodes constructed in python, the turtlebots are sent velocity and turn-rate commands individually and the experimental data is recorded on a master computer running ROS. The robot computers are setup as slave and the master computer connects to all the robots over a WiFi network. The experiment is performed using real-range measurements from the Decawave sensors which are setup as anchor and tag based on the vehicle which is measuring the range. The sensors provide accurate range measurements up to 10m but are prone to multi-path errors and interference from electromagnetic fields in its immediate vicinity. The codes for this experiment are available on github at **Github Code** and the experimental video is available on youtube at **Experimental Video**. The parameters used in the hardware experiment are listed in Table 4.

A closer look at the pairwise trajectories between vehicles **1** and **2** shows that they are moving closer, whereas vehicles **1** and **3** in Figure 13 are moving away from each other. From the observability analysis in Section III, it is clear that a gradual increase in range decreases the overall system observability. In this case, as the vehicles are moving away from each other, the range between them increases (seen in Figure 13) that reduces the overall system observability. As these are hardware systems, non-linearities develop in the robots from its natural wear and tear and are not always accounted for in the vehicle dynamics. This makes it important to choose proper trajectories such that there is enough variation in the range measurement.

As detailed in Section II, the states of a multi-vehicle cooperative relative framework is defined in (2). Figure 13 represents the global trajectory where **vehicle 1** is the central vehicle, and the pose of the other vehicles is estimated in vehicle 1's body frame. Due to physical space limitation in the Mocap area and network bandwidth constraints, three turtlebots are used in the hardware experiment. The results are represented in Figure 14, where solid lines represent the direct measurement localization (DML) and 3σ bounds, and dotted lines represent indirect measurement (IML) relative errors among the vehicle pairs. It is to be noted that MHEKF is used to initialize the filters, and around the 13-second mark (marked by a dotted vertical line), indirect range measurements are used in the estimation algorithm. Improvement with IML is not significantly visible in the hardware experiments due to certain logistical constraints like limited space in the experimental region (seen in Figure 12), the number of turtlebots used (3, in this case, to make sure there are no collisions in the available area) and not a significant variation of relative movement like the simulation. The relative geometry during the start of the N-vehicle filter is not ideal as well.

However, from Figure 14 and Table 5, it is evident that the overall error is reduced using IML. Given enough physical space and network bandwidths with a higher number of robots, hardware experiments will also show similar improvements as the simulation case. However, the results shown in Figure 14 are in accordance with the findings

This article has been accepted for publication in a future issue of this journal, but has not been fully edited. Content may change prior to final publication. Citation information: DOI 10.1109/ACCESS.2020.3035470, IEEE Access

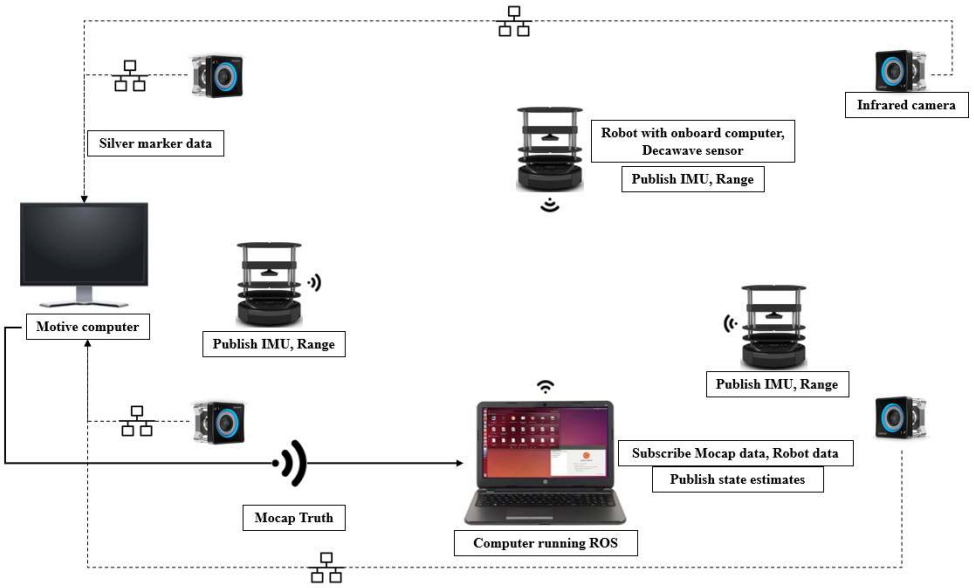

FIGURE 11: R.I.S.C Lab multi-vehicle test bed

Parameter	Multiple vehicles (Initialized with MHEKF
Range uncertainty	0.1 m (from Decawave)
Odometry uncertainty	[0.01 m/s, 0.005 rad/s]
Turtlebot Velocity	0.05 m/s

TABLE 4: Hardware parameters - Multiple Relative Localization for Figs 13- 14

in Section III. An increase in overall range measurement between vehicles **1** and **3** reduces the observability in the system as the uncertainty bounds in p_x between these two vehicles does not decrease over time whereas for vehicle pair **1** and **2**. The uncertainty bounds decrease for all states. Similarly, the variation in the range between vehicle pairs **1** and **2** is greater than vehicle pairs **1** and **3** which indicates a higher range rate that generally provides more information in the system. Based on these results, it is clear that the results obtained in the hardware experiment are commensurate with the simulations, and MHEKF can be used to initialize an N-vehicle system with no *a-priori* information. The main contributions of this paper are summarized in Section V, and discussions regarding some of the interesting future work using the results from the observability section are also provided.

V. CONCLUSION

In this paper, we have successfully solved a relative cooperative navigation problem with no *a-priori* information. Simulation results in Section II and hardware results in Section IV demonstrate that an N-vehicle cooperative filter can be initialized using limited computation capabilities when no *a priori* information is available. This cooperative filter is initialized by leveraging the outputs from the multiple pairwise filters using the MHEKF. A nonlinear observability analysis using Lie derivatives was performed to provide analytical conditions for observability of the pairwise and the cooperative cases. Those observability constraints were then used to select effective vehicle trajectories which were demonstrated to improve filter performance both in simulation and in hardware. Real-time hardware experiments were conducted using multiple ROS-based platforms consisting of Turtlebots, Decawave ranging sensors, and on-board processors for real-time demonstration of the multi-agent initialization and filter performance.

In the future, the MHEKF technique will be used for various applications to demonstrate its advantage. Cost functions based on (19) will be developed to provide optimized vehicle trajectories given the vehicle and sensor characteristics and limitations. The filter will also be adapted for use in a batch framework to improve robustness to communication delays and dropouts.

REFERENCES

[1] National Aeronautics and Space Administration. URBAN AIR MOBILITY (UAM) MARKET STUDY. https://www.nasa.gov/sites/default/files/atoms/files/uam-market-study-executive-summary-v2.pdf. [Online; accessed 7-Jun-2020].

[2] National Aeronautics and Space Administration. NASA and Uber Test System for Future Urban Air Transport. https://www.nasa.gov/feature/ames/nasa-and-uber-test-system-for-future-urban-air-transport. [Online; accessed 7-Jun-2020].

[3] CNET RoadShow. Hyundai and Uber

This article has been accepted for publication in a future issue of this journal, but has not been fully edited. Content may change prior to final publication. Citation information: DOI 10.1109/ACCESS.2020.3035470, IEEE Access

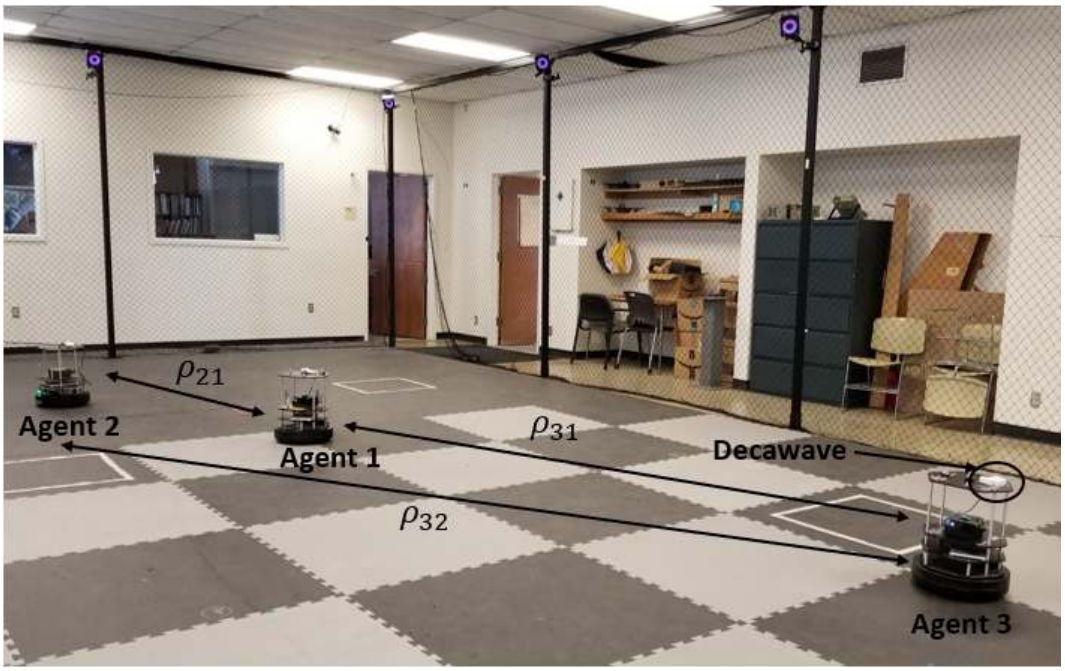

FIGURE 12: Experimental Setup - Multiple turtlebots with Decawave sensors with MOCAP as the indoor GPS system

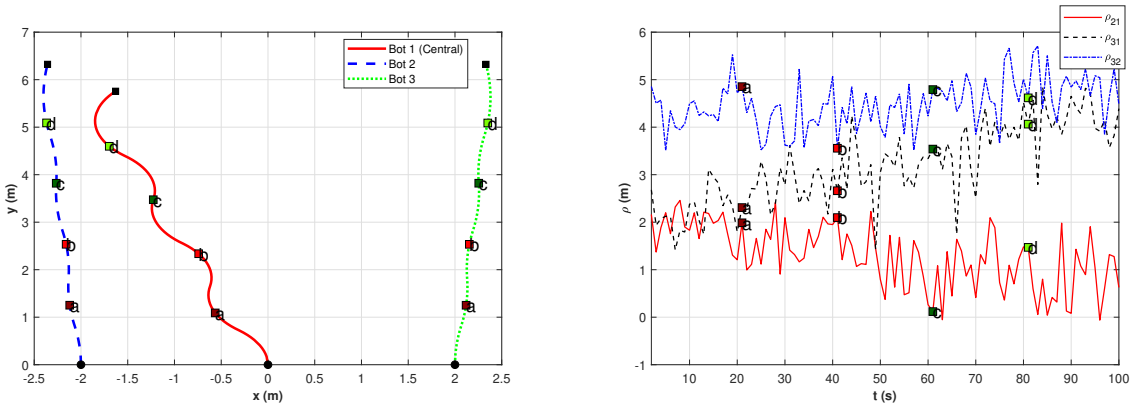

FIGURE 13: Hardware Setup - True trajectories (Left) & Range measurement (Right)

-	**Avg.** p_x **(m)**	**IML -** p_x **(m)**	**DML -** p_x **(m)**	**Avg.** p_y **(m)**	**IML -** p_y **(m)**	**DML -** p_y **(m)**	**IML -** $\delta\psi$ **(deg)**	**DML -** $\delta\psi$ **(deg)**
p_{21}	-0.39	0.04	0.08	-1.21	0.07	0.16	2.60	3.60
p_{31}	-0.06	0.05	0.07	-4.40	0.06	0.13	1.27	1.77

TABLE 5: Cooperative relative localization - RMS Errors (HW)

Elevate debut urban air taxi concept S-A1. https://www.cnet.com/roadshow/news/hyundai-uber-elevate-urban-air-taxi-ces-2020/. [Online; accessed 7-Jun-2020].

[4] David P Thipphavong, Rafael Apaza, Bryan Barmore, Vernol Battiste, Barbara Burian, Quang Dao, Michael Feary, Susie Go, Kenneth H Goodrich, Jeffrey Homola, et al. Urban air mobility airspace integration concepts and considerations. In 2018 Aviation Technology, Integration, and Operations Conference, page 3676, 2018.

[5] Christopher Silva, Wayne R Johnson, Eduardo Solis, Michael D Patterson, and Kevin R Antcliff. Vtol urban air mobility concept vehicles for technology development. In 2018 Aviation Technology, Integration, and Operations Conference, page 3847, 2018.

[6] Xuxi Yang and Peng Wei. Autonomous on-demand free flight operations in urban air mobility using monte carlo tree search. In International Conference on Research in Air Transportation (ICRAT), Barcelona, Spain, 2018.

[7] Jonas Lundberg, Mattias Arvola, Carl Westin, Stefan

This article has been accepted for publication in a future issue of this journal, but has not been fully edited. Content may change prior to final publication. Citation information: DOI 10.1109/ACCESS.2020.3035470, IEEE Access

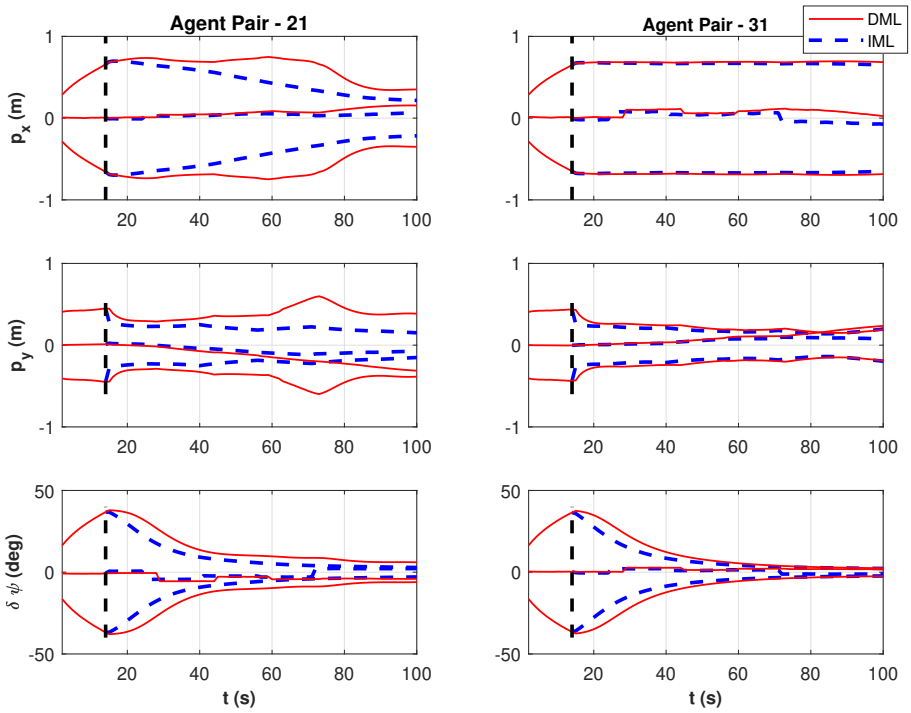

FIGURE 14: Hardware - Error with 3σ bounds for multi-vehicle scenario. The trajectory followed is represented in Figure 13

Holmlid, Mathias Nordvall, and Billy Josefsson. Cognitive work analysis in the conceptual design of first-of-a-kind systems–designing urban air traffic management. Behaviour & Information Technology, 37(9):904–925, 2018.

[8] Claire Tomlin, George J Pappas, and Shankar Sastry. Conflict resolution for air traffic management: A study in multiagent hybrid systems. IEEE Transactions on automatic control, 43(4):509–521, 1998.

[9] Sohum Misra, Bingyu Wang, Kaarthik Sundar, Rajnikant Sharma, and Sivakumar Rathinam. Single vehicle localization and routing in gps-denied environments using range-only measurements. IEEE Access, 8:31004–31017, 2019.

[10] Seung-Hyun Kong, José A López-Salcedo, Yuanxin Wu, and Euiho Kim. Ieee access special section editorial: Gnss, localization, and navigation technologies. IEEE Access, 7:131649–131652, 2019.

[11] Lingxuan Hu and David Evans. Localization for mobile sensor networks. In Proceedings of the 10th annual international conference on Mobile computing and networking, pages 45–57, 2004.

[12] Motilal Agrawal and Kurt Konolige. Real-time localization in outdoor environments using stereo vision and inexpensive gps. In 18th International conference on pattern recognition (ICPR'06), volume 3, pages 1063–1068. IEEE, 2006.

[13] Giulio Reina, Andres Vargas, Keiji Nagatani, and Kazuya Yoshida. Adaptive kalman filtering for gps-based mobile robot localization. In 2007 IEEE International Workshop on Safety, Security and Rescue Robotics, pages 1–6. IEEE, 2007.

[14] Shengming Chang, Youming Li, Hui Wang, Wenfei Hu, and Yongqing Wu. Rss-based cooperative localization in wireless sensor networks via second-order cone relaxation. IEEE Access, 6:54097–54105, 2018.

[15] Chengjiao Sun, Yonggang Zhang, Guoqing Wang, and Wei Gao. A maximum correntropy divided difference filter for cooperative localization. IEEE Access, 6:41720–41727, 2018.

[16] Shiwa Chen, Jianyun Zhang, and Chengcheng Xu. Robust distributed cooperative localization with nlos mitigation based on multiplicative convex model. IEEE Access, 7:112907–112920, 2019.

[17] Shaoxing Hu, Chunpeng Chen, Aiwu Zhang, Weidong Sun, and Linlin Zhu. A small and lightweight autonomous laser mapping system without gps. Journal of Field Robotics, 30(5):784–802, 2013.

[18] Ruijie He, Sam Prentice, and Nicholas Roy. Planning in information space for a quadrotor helicopter in a gps-denied environment. In 2008 IEEE International Conference on Robotics and Automation, pages 1814–1820. IEEE, 2008.

[19] András L Majdik, Damiano Verda, Yves Albers-Schoenberg, and Davide Scaramuzza. Air-ground matching: Appearance-based gps-denied urban local-

ization of micro aerial vehicles. Journal of Field Robotics, 32(7):1015–1039, 2015.

[20] Martin Saska, Jan Vakula, and Libor Přeućil. Swarms of micro aerial vehicles stabilized under a visual relative localization. In 2014 IEEE International Conference on Robotics and Automation (ICRA), pages 3570–3575. IEEE, 2014.

[21] Martin Saska. Mav-swarms: unmanned aerial vehicles stabilized along a given path using onboard relative localization. In 2015 International Conference on Unmanned Aircraft Systems (ICUAS), pages 894–903. IEEE, 2015.

[22] Richard Matthaei, Gerrit Bagschik, and Markus Maurer. Map-relative localization in lane-level maps for adas and autonomous driving. In 2014 IEEE Intelligent Vehicles Symposium Proceedings, pages 49–55. IEEE, 2014.

[23] Rajnikant Sharma and Daniel Pack. Cooperative sensor resource management for multi target geolocalization using small fixed-wing unmanned aerial vehicles. In AIAA Guidance, Navigation, and Control (GNC) Conference, pages 1–11, 2013.

[24] Anusna Chakraborty, Clark N Taylor, Rajnikant Sharma, and Kevin M Brink. Cooperative localization for fixed wing unmanned aerial vehicles. In 2016 IEEE/ION Position, Location and Navigation Symposium (PLANS), pages 106–117. IEEE, 2016.

[25] Anusna Chakraborty, Rajnikant Sharma, and Kevin Brink. Cooperative localization for multi-rotor uavs. In AIAA Scitech 2019 Forum, page 0684, 2019.

[26] Rajnikant Sharma, Randy W Beard, Clark N Taylor, and Stephen Quebe. Graph-based observability analysis of bearing-only cooperative localization. Robotics, IEEE Transactions on, 28(2):522–529, 2012.

[27] Anusna Nikita Mishra, Chakraborty, Rajnikant Sharma, and Kevin Brink. Cooperative relative pose estimation to aid landing of an unmanned aerial vehicle on a moving platform. In 2019 Indian Control Conference (ICC). IEEE, 2019.

[28] Brandon Araki, Igor Gilitschenski, Tatum Ogata, Alex Wallar, Wilko Schwarting, Zareen Choudhury, Sertac Karaman, and Daniela Rus. Range-based cooperative localization with nonlinear observability analysis. In 2019 IEEE Intelligent Transportation Systems Conference (ITSC), pages 1864–1870. IEEE, 2019.

[29] Zongwen Xue and Howard Schwartz. A comparison of several nonlinear filters for mobile robot pose estimation. In 2013 IEEE International Conference on Mechatronics and Automation, pages 1087–1094. IEEE, 2013.

[30] BG Sileshi, Carles Ferrer, and Joan Oliver. Particle filters and resampling techniques: Importance in computational complexity analysis. In 2013 Conference on Design and Architectures for Signal and Image Processing, pages 319–325. IEEE, 2013.

[31] Sanjeev Arulampalam and Branko Ristic. Comparison of the particle filter with range parameterized and modified polar ekf's for angle-only tracking. In Proc. Spie, volume 4048, pages 288–299, 2000.

[32] He Bai and Randal W Beard. Relative heading estimation for target handoff in gps-denied environments. In 2016 American Control Conference (ACC), pages 336–341. IEEE, 2016.

[33] Anusna Chakraborty, Kevin Brink, Rajnikant Sharma, and Laith Sahawneh. Relative pose estimation using range-only measurements with large initial uncertainty. In 2018 Annual American Control Conference (ACC), pages 5055–5061. IEEE, 2018.

[34] Patric Jensfelt and Steen Kristensen. Active global localization for a mobile robot using multiple hypothesis tracking. IEEE Transactions on Robotics and Automation, 17(5):748–760, 2001.

[35] Loris Bazzani, Domenico Bloisi, and Vittorio Murino. A comparison of multi hypothesis kalman filter and particle filter for multi-target tracking. In Performance Evaluation of Tracking and Surveillance workshop at CVPR, pages 47–54, 2009.

[36] Yongkyu Song and Jessy W Grizzle. The extended kalman filter as a local asymptotic observer for nonlinear discrete-time systems. In American Control Conference, 1992, pages 3365–3369. IEEE, 1992.

[37] Robert Hermann and Arthur J Krener. Nonlinear controllability and observability. IEEE Transactions on automatic control, 22(5):728–740, 1977.

[38] Gianluca Antonelli, Filippo Arrichiello, Stefano Chiaverini, and Gaurav S Sukhatme. Observability analysis of relative localization for auvs based on ranging and depth measurements. In Robotics and Automation (ICRA), 2010 IEEE International Conference on, pages 4276–4281. IEEE, 2010.

[39] He Bai and Randal W Beard. Relative heading estimation and its application in target handoff in gps-denied environments. IEEE Transactions on Control Systems Technology, 2017.

[40] Decawave. DWM1000 Module. https://www.decawave.com/product/dwm1000-module/. [Online; accessed 29-Oct-2018].

[41] Chao Gao, Guorong Zhao, and Hassen Fourati. Cooperative Localization and Navigation: Theory, Research, and Practice. CRC Press, 2019.

[42] Randal W Beard and Timothy W McLain. Small unmanned aircraft: Theory and practice. Princeton university press, 2012.

[43] Pavel Ivanov, Simo Ali-Löytty, and Robert Piché. Evaluating the consistency of estimation. In International Conference on Localization and GNSS 2014 (ICL-GNSS 2014), pages 1–5. IEEE, 2014.

[44] Wolfgang Niehsen. Information fusion based on fast covariance intersection filtering. In Proceedings of the Fifth International Conference on Information Fusion. FUSION 2002.(IEEE Cat. No. 02EX5997), volume 2, pages 901–904. IEEE, 2002.

[45] TurtleBot. Turtlebot 2. https://www.turtlebot.com/. [Online; accessed 19-Nov-2018].

ANUSNA CHAKRABORTY completed her B.Tech. degree in Electrical Engineering from St.Thomas's College of Engineering and Technology, Kolkata, India in 2012. She is currently pursuing her Ph.D. in Aerospace Engineering at University of Cincinnati, Ohio, USA from 2017 where she is a Graduate Research Assistant in the R.I.S.C Lab. Anusna has 11 technical publications. She is working on estimation and path planning problems in GPS-denied or restricted environments. Her research interests are sensor fusion, controls, path planning, navigation, robotics and autonomous robots

DR. KEVIN M. BRINK is a Senior Research Engineer and the Technical Lead for the Navigation and Estimation Team at the Air Force Research Laboratory, Munitions Directorate, Eglin AFB, FL. He has a background in Mathematics and Electrical Engineering and his research focuses primarily on single and multi-agent navigation in GPS-degraded/denied environments.

RAJNIKANT SHARMA received the B.E. degree in Electrical Engineering from the University of Rajasthan, Jaipur, India, in 2003, the M.E. degree in Aerospace Engineering from the Indian Institute of Science, Bangalore, India, in 2005, and the Ph.D. degree in Electrical Engineering in 2011 from the Brigham Young University, Provo, UT. Currently, he is an Assistant Professor in the Aerospace and Engineering Mechanics Department at the University of Cincinnati. In 2011–2013, he was a Postdoctoral fellow at Center for UAS Research, US Air Force Academy, Colorado. From 2005–2007, he was a Scientist B at the Center for Airborne Systems, Defense Research and Development Organization, Ministry of Defense, Bangalore, India. His primary research interests are guidance, navigation, and control of unmanned aerial vehicles and multiple vehicle coordination, control, and localization. He is a member of the IEEE and AIAA community.